Temperature and Pressure Dependence of High-Resolution Air-Broadened Absorption Cross Sections of NO₂ (415−525 nm)

S. A. Nizkorodov*,†

Arthur Amos Noyes Laboratory of Chemical Physics, California Institute of Technology, Pasadena, California 91125

S. P. Sander* and L. R. Brown*

Jet Propulsion Laboratory, California Institute of Technology, 4800 Oak Grove Drive, Pasadena, California 91109

Cross sections of air-broadened NO₂ in the 415−525 nm region are reported. These are retrieved from 21 absorption spectra recorded at 0.060 cm⁻¹ resolution with the McMath−Pierce Fourier Transform Spectrometer located on Kitt Peak in Arizona. The measurements are obtained for pressures (1−760 Torr) and temperatures (220−298 K) that are representative of typical tropospheric and stratospheric conditions. Two sigma uncertainty (95% confidence interval ≈ $2\sigma_{mean}$) for the absolute absorption cross sections is below ±7% over the reported wavelength range. The average integrated intensity of all our data is $\langle\sigma\rangle_{400-500\,nm} = 4.53 \times 10^{-17}$ cm² nm, which is within 0.2% of the averaged value from the recent literature. The wavelength (referred to vacuum) accuracy is 0.011 cm⁻¹ (2.8×10^{-4} nm at 500 nm) and precision is 0.0022 cm⁻¹ throughout the investigated wavelength range. In agreement with previous observations, high-resolution features in the NO₂ absorption spectrum display a strong pressure dependence with an effective pressure broadening parameter of 0.116 ± 0.003 cm⁻¹/atm (the rate of increase of Lorentzian half width at half-maximum with pressure). Temperature has a relatively minor effect on the shapes of individual high-resolution features, but it exerts a complex dependence on the relative line intensities. Absorption cross sections reported here represent the highest resolution data available over a substantial (>100 nm) wavelength range for quantitative analysis of NO₂ atmospheric column absorption spectra.

I. Introduction

Nitrogen dioxide is a trace species that plays several important roles throughout the atmosphere. Photodissociation of NO₂ is a key process in the photochemical chain mechanism that forms ozone in the background and polluted regions of the troposphere. In high concentrations, NO₂ can cause severe adverse health effects and is classified by the U. S. Environmental Protection Agency as a "criteria pollutant". In the stratosphere, NO₂ participates in catalytic cycles that both form and destroy ozone, and it couples with species in the HO_x, ClO_x, and BrO_x radical families that significantly affect the ozone budget. The importance of NO₂ chemistry has motivated numerous studies of the global distribution, sources and sinks of NO₂ in the atmosphere.[1] Since UV−visible spectroscopy is frequently used to monitor NO₂ by remote sensing, its absorption spectrum must be accurately characterized for all relevant atmospheric conditions.[2,3]

From the perspectives of molecular spectroscopy, nitrogen dioxide occupies a unique position between small molecules with well-defined energy level structure and large molecules with a quasi-continuum of coupled energy levels. In the language of radiationless transition theory,[4] nitrogen dioxide, with its anomalously long fluorescence lifetime,[5] is a "sparse intermediate case" molecule.[6] Its sizable density of states, strong coupling between the ground electronic state ($^2A_1$) and excited states ($^2B_1$, $^2B_2$, $^2A_2$), and large geometrical difference in the potential energy surfaces of the lowest electronic states[7,8] make the visible spectrum of NO₂ too congested to assign, thus far. Even when cooled to supersonic temperatures, the spectrum contains hundreds of vibronic bands throughout the entire visible range.[9,10] Spectroscopic work on this molecule has always been driven by a conviction that higher resolution spectra will aid in understanding the dynamics and spectroscopy of this intriguing molecule. Reference 11 provides a complete historical perspective on NO₂ spectroscopy from 1834 to 1978; more recent references can be found in ref 3.

The room-temperature absorption spectrum of NO₂ looks like a 150 nm wide (fwhm), slightly asymmetric "blob" centered at about 400 nm and covered by thousands of reproducible "lines",[2] most of which have no definite spectroscopic assignment. From the standpoint of atmospheric remote sensing, however, a catalog of the pressure and temperature-dependent absorption cross sections over the broadest possible spectral range and at the highest possible resolution is perhaps more valuable than a detailed assignment of the spectrum.[3] The existing NO₂ absorption cross sections are quite adequate for remote sensing under low spectral resolution. However, low-temperature studies of high-resolution absorption cross sections of NO₂ are limited, and pressure dependence studies are just beginning to emerge.[12−15]

* To whom correspondence should be addressed. (Nizkorodov) nizkorod@uci.edu; (Sander) Stanley.P.Sander@jpl.nasa.gov; (Brown) linda.brown@jpl.nasa.gov.
† Present address: Department of Chemistry, University of California at Irvine, Irvine, CA 92697, USA.

TABLE 1: Previous Studies of NO$_2$ Absorption Cross Sections[a]

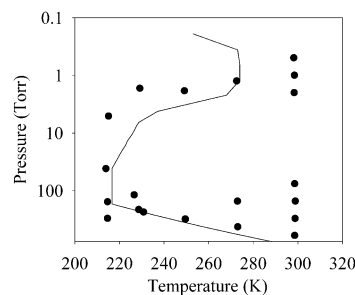| ref	wavelength range (nm)	resolution (cm^{-1})	P (Torr)	T (K)	no. of spectra
this work	415−525	0.060[a]	1−760	215, 230, 250, 273, 298	21
13	385−725	0.1[b]	0.007−760	220, 240, 294	24
14	250−800	0.5	76, 760	223, 246, 260, 280, 293	10
18	360−470	0.15	0.5−3.0	298	1
12	350−585	0.15[c]	100, 600	217, 230, 240, 294	6
17	441−452	0.028[c]	5−600	240, 298	8
19	330−670	2.0	10	298	1
20	270−500	0.5	low[d]	200 ± 20	1
21	400−500	0.5	0.01−35	220, 240	4
22	300−500	0.5	0.01−35	298	2
23	200−700	2.0	2−60	298	1

[a] Only measurements overlapping with the 415−525 nm range and using resolution better than 2 cm^{-1} are included in this table. See refs 2,22 for more complete listings. The total number of reported combinations of P,T conditions is listed in the last column. [a] Resolution is defined as 0.604/MOPD, where MOPD is the maximum optical path difference of the FT instrument. This resolution is appropriate for the boxcar apodization. [b] Resolution is defined as 0.9/MOPD. [c] Resolution is defined as 0.5/MOPD. [d] This is a jet experiment with a near collision-free environment.

In fact, the spectral resolution has been limited by the instrument in all but a few studies. The main goals of this work are to improve the database of NO$_2$ absorption cross sections from the standpoint of spectral resolution, absolute accuracy, pressure and temperature dependences, and wavelength calibration and to make these data available to the spectroscopic and atmospheric scientific communities, through spectroscopic databases such as HITRAN.[16]

The Ozone Monitoring Instrument (OMI) that will be launched on the Earth Observing System Aura spacecraft in 2004 will measure global NO$_2$ column abundances from nadir observations of reflected solar radiation. Accurate validation of space measurements can be done from the ground using direct solar absorption measurement at high spectral resolution.[17] The present wavelength range (415−525 nm) is characterized by highly structured absorptions in the NO$_2$ spectrum, and it will be useful for the OMI validation. Specifically, OMI uses a spectral window from 405 to 465 nm for NO$_2$. Their theoretical basis document states that the 430−450 nm region is where the most precise fits are obtained for NO$_2$.

Table 1 is a summary of the previous measurements of NO$_2$ absolute absorption cross sections carried out over the spectral range of interest (415−525 nm) using high to moderately high resolution (<2 cm^{-1}).[12−14,18−23] Present experimental conditions correspond to 0.060 cm^{-1} instrumental bandwidth (defined as 1.207/(2 × MOPD), where MOPD stands for maximum optical path difference). Pressure dependent measurements of NO$_2$ cross sections at 0.028 cm^{-1} resolution were obtained at 240 and 300 K over a narrow wavelength range by Wennberg et al.[17] These spectra were discussed further in ref 12. Vandaele et al.[13] recently reported near-infrared and visible cross sections of NO$_2$ at stated resolutions of 0.05 and 0.1 cm^{-1}, respectively. All other researchers used instrumental resolutions that are lower than 0.1 cm^{-1} in their studies. It is possible that even 0.060 cm^{-1} resolution may still be insufficient to fully resolve the spectrum (Doppler width for NO$_2$ is fwhm = 0.036 cm^{-1} at 500 nm and 298 K), but a large fraction of the observed spectrum appears to be almost invariant with respect to the resolution.

As seen in Figure 1, we succeeded in covering a substantial portion of the P, T grid characteristic of conditions in the

Figure 1. Grid of pressures and temperatures used in this work (dots) compared to the conditions found in a standardized atmosphere (line). One of the objectives of this work was to cover the widest pressure and temperature range relevant for the atmosphere.

TABLE 2: Summary of Experimental Conditions for the High-Resolution Spectra of NO$_2$ Recorded in This Work[a]

P (Torr)	T (K)	[NO$_2$] (molecule/cm^3)	[N$_2$O$_4$] (molecule/cm^3)	% error in [NO$_2$]	correction
596.10	298.6	1.33 × 10^{15}	4.82 × 10^{11}	4.9	0.966
302.20	298.8	1.33 × 10^{15}	4.76 × 10^{11}	4.9	0.957
151.00	298.9	1.34 × 10^{15}	4.77 × 10^{11}	4.9	1.012
75.45	298.6	1.32 × 10^{15}	4.75 × 10^{11}	4.9	1.069
1.99	298.4	3.01 × 10^{15}	2.51 × 10^{12}	2.7[a]	1.057
0.49	298.2	7.51 × 10^{14}	1.58 × 10^{11}	2.7[a]	1.104
760.50	273.2	2.07 × 10^{15}	9.20 × 10^{12}	4.9	0.942
421.50	273.0	2.01 × 10^{15}	8.83 × 10^{12}	4.9	0.974
151.20	272.9	1.77 × 10^{15}	6.93 × 10^{12}	4.9	0.966
1.24	272.6	2.05 × 10^{15}	9.57 × 10^{12}	2.7[a]	1.006
309.50	249.6	1.53 × 10^{15}	4.98 × 10^{13}	4.7	1.014
309.00	249.5	1.53 × 10^{15}	5.05 × 10^{13}	4.7	0.974
1.85	249.2	2.97 × 10^{15}	1.97 × 10^{14}	2.5[a]	1.026
233.80	230.8	1.67 × 10^{15}	5.18 × 10^{14}	3.8	1.047
211.30	228.7	1.41 × 10^{15}	4.89 × 10^{14}	3.8	1.114
117.84	226.6	1.37 × 10^{15}	6.01 × 10^{14}	3.7	0.986
1.67	229.2	1.81 × 10^{15}	7.48 × 10^{14}	2.4[a]	1.079
300.50	214.7	1.58 × 10^{15}	4.07 × 10^{15}	3.5	0.900
155.30	214.7	1.61 × 10^{15}	4.24 × 10^{15}	3.5	0.946
41.27	214.0	1.61 × 10^{15}	4.66 × 10^{15}	3.5	0.921
5.07	215.1	1.72 × 10^{15}	4.49 × 10^{15}	2.7[a]	1.009

[a] Partitioning between NO$_2$ and N$_2$O$_4$ is calculated using equilibrium constant from ref 27. Errors in [NO$_2$] (95% confidence limits) are calculated as described in the text. Combination of the latter with estimated uncertainties in absolute absorbances (<4.3 %) results in <7% uncertainty in the reported absorption cross sections. The last column lists the correction factors by which the raw cross sections were multiplied in order to force the integrated value in the 435−500 nm window to be the same for all P,T data sets (2.489 × 10^{-17} cm^2 nm, which is the average of all individual $\langle\sigma\rangle_{435-500}$ values displayed in Figure 6). [a] Measurements done using undiluted NO$_2$/air mixture (no error from the flows).

"standard" troposphere and stratosphere. As discussed below, our data fully support the pronounced effect of pressure on the visible absorption cross sections of NO$_2$, which was first discovered in ref 12 and verified in refs 13−14.

II. Experimental Details

Absorption spectra of NO$_2$/air mixtures were obtained from July 9 to July 13, 2001 with the McMath−Pierce Fourier transform spectrometer (FTS) at the National Solar Observatory located at Kitt Peak. Table 2 is a summary of the gas sample conditions for 21 spectra recorded at 0.060 cm^{-1} resolution (see below). A schematic diagram of the experimental setup is shown in Figure 2. A 300 W xenon arc lamp was used as a broadband light source. The lamp spectrum was trimmed with a combination of BG23 UV band-pass and GG385 long-pass filters, which efficiently attenuated wavelengths below 400 nm and prevented NO$_2$ photolysis in the cell. The FTS spectrometer was equipped with an internal CuSO$_4$ liquid filter[24] to further limit the
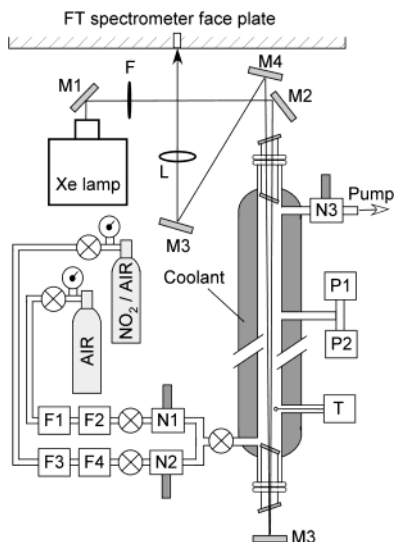
Figure 2. Schematic diagram of the experimental setup. Broadband UV radiation from a 300W Xe lamp is sent into a 201 cm long cell with mirrors M1 and M2. Filters, F, are used to restrict the wavelength range to 400−600 nm; both to minimize NO_2 photolysis in the cell and to reduce noise on the detector. Radiation passes through the cell twice and is steered onto the FTS 8 mm input aperture with mirrors M3-M5 and lens L. The cell has a jacket cooled by circulating methanol. Gases enter the cell through calibrated flow meters, F1−F4, and needle valves, N1 and N2. The pressure in the cell is controlled with N3 and measured with two calibrated capacitance manometers, M1 and M2. Temperature of the gas flow is probed with a K-type thermocouple, T.

bandwidth of detected radiation. The radiation was allowed to pass through the sample cell twice and then it was weakly focused on the 8 mm FTS input aperture, overfilling it by a factor of 2.5. Two matched silicon photodiode detectors were used.

The absorption cell was a 2.5 cm diameter precision glass tube encapsulated in a 7.5 cm diameter cooling jacket circulating chilled methanol to achieve gas temperatures down to 210 K. It was fully wrapped in insulating foam to improve the temperature uniformity. To prevent frosting, each end of the cell was sealed with a double window insert equipped with an evacuated supporting tube between the windows. The cell measured 201 ± 0.2 cm in length between the inner windows of the two inserts. Pressure inside the cell was measured in the middle with two capacitance manometers rated at 10 and 1000 Torr. The manometers were carefully calibrated against standards to better than 0.1% accuracy both before and after the measurement. Temperature in the cell was measured about 10 cm downstream from the point of gas entry with a calibrated K-type thermocouple. The temperature of the cooling fluid was typically 1−5 K lower than the measured gas temperature, with the difference increasing at lower temperatures and larger gas loads. The effective measurement temperature was taken as an average of the coolant temperature and gas temperature at the cell entrance resulting in an average uncertainty of ±2 K.

The gas mixtures were prepared by mixing a flow of synthetic air with a flow of a commercial gravimetric NO_2/air mixture with a stated molar NO_2 fraction of $\delta = 5.00\%$. Each flow was simultaneously measured by two flow meters arranged in series (100 and 1000 sccm for air; 10 and 50 sccm for the NO_2/air mixture). The flow meters were absolutely calibrated using two independent techniques: (i) measurement of the rate of gas volume increase vs flow at constant pressure; and (ii) measurement of the rate of pressure increase vs flow in a calibrated volume. The calibration was further verified by cross-calibrating
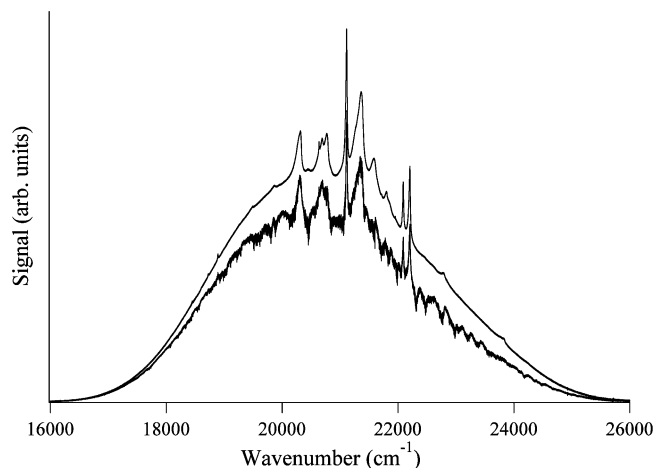

Figure 3. Sample experimental spectra. Background spectrum (top) was obtained with pure N_2 in the cell. Structure in the background is characteristic of Xe arc lamp emission. The emission spectrum is truncated by filters (Figure 2) on both blue and red sides. Sample spectrum (bottom) was taken for $[NO_2] = 1.33 \times 10^{15}$ molecule/cm³; $P_{total} = 302.2$ Torr and $T = 298.8$ K. Each spectrum resulted from co-adding 15 interferograms at 0.060 cm^{-1} resolution. The high-frequency modulations in the spectrum are indigenous to NO_2. For the range of 18 000 to 24 000 cm^{-1}, RMS noise in the resulting (base e) absorbance was below 0.005, which, in combination with other factors, limited the accuracy of the reported cross sections to better than 7% (see text).

the flow meters connected in series. Both gas flows, as well as the total cell pressure, could be independently controlled with a set of three in-line needle valves (see Figure 2). The concentration of NO_2 in the cylinder was independently verified right after the measurement by UV spectophotometry using calibration against vacuum-distilled NO_2 samples. This measurement resulted in a molar fraction of $\delta = 4.70 \pm 0.05\%$, suggesting that either gravimetric fraction specified by the manufacturer was incorrect or NO_2 mixture was slowly aging (it was received several months prior to the experiment). Concentration of NO_2 was measured again with FTIR spectroscopy, 12 months after the measurement, yielding an even lower fraction and confirming that aging was responsible for the discrepancy. We have adopted our value of $\delta = 4.70 \pm 0.12\%$ for the molar fraction of NO_2 for the analysis presented here, with the increased uncertainties reflecting the maximal possible effect of aging.

Spectra were recorded over the range of 15 000−30 000 cm^{-1} at 0.060 cm^{-1} spectral resolution (1.207/[2 × MOPD] for 10 cm MOPD, double-sided interferograms, and boxcar apodization), with the data points in the frequency domain files spaced by 0.0286 cm^{-1} (corresponding to Nyquist resolution of 0.057 cm^{-1}). Because of the spectral filtering, 99% of the radiation reaching the detector was confined to 17 000−25 000 cm^{-1} window (Figure 3). The cross sections were calculated for the entire range but they are expected to be accurate (see below) only between ∼19 000−24 000 cm^{-1} (ca. 415−525 nm). Fifteen interferograms were co-added with a total acquisition time of about 80 min for each T, P point. To save time, background scans, which were taken between all sample spectra, were recorded at a reduced resolution of 0.2 cm^{-1} and interpolated to match the data spacing in the sample spectra. This procedure is fully justified because all features in the Xe-lamp emission spectrum (Figure 3) are all substantially wider than 10 cm^{-1}. We also recorded background spectra at the 0.060 cm^{-1} resolution to confirm that they are identical to the interpolated lower resolution scans. For each scan, a detailed log, raw

interferogram, and transformed spectrum were saved on disk for subsequent analysis.

The FTS wavelength refers to the vacuum scale. To confirm the absolute frequency accuracy of the FTS (0.01 cm^{-1}) a reference cell containing I$_2$[25] was periodically inserted in the optical path (specifically during the 27th, 44th, and 54th scans). The first spectrum was iodine alone, whereas the last two were obtained with NO$_2$ in the other cell. Observed line centers were retrieved by least-squares curve fitting of the unapodized spectrum[26] in less crowded intervals between 18 050 and 19 670 cm^{-1}. Stronger lines separated by more than 0.08 cm^{-1} from other features were compared, and some 300 empirical line centers from each spectrum were found to agree with each other with an RMS (root-mean-square) value of 0.0022 cm^{-1}. This was taken as evidence that the alignment of the FTS remained stable during the experiment and that the level of agreement represented the general precision of the wavenumber scale. However, the comparisons of observed values with calculated I$_2$ positions were worse; the RMS values ranged from 0.0038 to 0.0059 cm^{-1}. Calibration factors were computed as the average ratio between calculated and observed values. For example, using from 149 to 250 transitions from spectra #44 and #54, the factors were, respectively, 0.999 999 818 (316) and 0.999 999 850 (289). It can be seen that the uncertainty of the factors (in parentheses) is too large to justify their use, however. For example, the calibration factor would cause a difference of −0.004 cm^{-1} ± 0.0108 cm^{-1} at 22 000 cm^{-1}. Therefore, no calibration factors were applied to the cross section data. We conclude that the absolute accuracies of the wavenumber scale are 0.011 cm^{-1} with precisions of 0.0022 cm^{-1}. Harder et al., using the same FTS, calibrated their spectra based on 46 I$_2$ transitions from Gerstenkorn et al.[25] Their stated wavelength accuracy was 0.0002 nm at 400 nm or 0.011 cm^{-1}. In Figure 4, we plot our resulting cross sections against theirs and see good agreement within our stated accuracies.

III. Data Analysis

A. Uncertainties. Absorption cross sections are derived from measurements of wavelength-dependent absorbance, $A_\lambda = \ln(I_0/I)$, concentration of analyte, [NO$_2$], and absorption path length, L, related through the Lambert−Beer law

$$\sigma = \frac{A_\lambda}{[\text{NO}_2]L} \qquad (1)$$

The uncertainty in the absorption cross sections can be estimated via the standard propagation of errors, $\Delta\sigma/\sigma = \sqrt{(\Delta A/A)^2 + (\Delta[\text{NO}_2]/[\text{NO}_2])^2 + (\Delta L/L)^2}$. Minimizing uncertainties requires a careful balance of experimental conditions; one needs to keep the NO$_2$ density high enough to ensure accurate measurement of the absorbance, but low enough to avoid extensive dimerization of NO$_2$ at low temperatures. The following paragraphs separately describe contributions of experimental uncertainties in A_λ and [NO$_2$] to the total error. The path length uncertainty is negligibly small (0.1%) compared to the uncertainties in A_λ and [NO$_2$]. (Note, all numerical uncertainties used in this paper refer to 95% confidence intervals, which should be roughly equal to $2\sigma_{\text{mean}}$ for sufficiently large data sets).

The situation with NO$_2$ is somewhat complicated by its well-known dimerization reaction

$$\text{N}_2\text{O}_4 \leftrightarrow \text{NO}_2 + \text{NO}_2 \qquad (2)$$
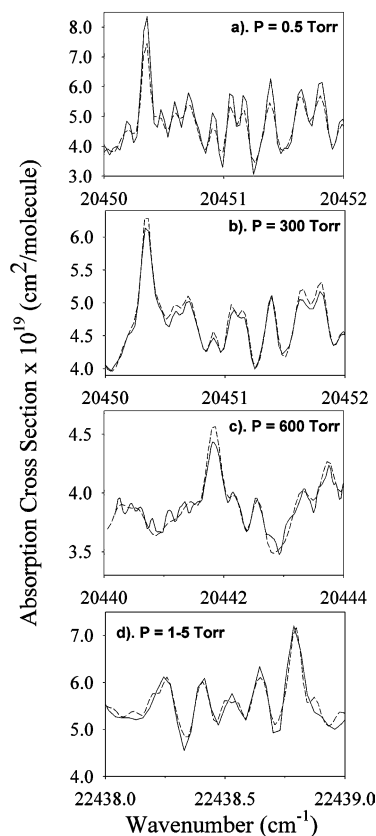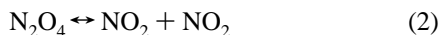

Figure 4. Comparison between absolute cross sections reported by this (solid line) and other (broken line) research groups. (a). This work (T = 298 K, P = 0.49 Torr, Res. = 0.060 cm^{-1}) vs data of Vandaele et al.[13] (294 K, 0.05 Torr, 0.1 cm^{-1}). (b). This work (298 K, 302 Torr, 0.06 cm^{-1}) vs data of Vandaele et al.[13] (294 K, 300 Torr, 0.1 cm^{-1}). (c). This work (298 K, 596 Torr, 0.060 cm^{-1}) vs data of Harder et al.[12] (294 K, 600 Torr, 0.15 cm^{-1}). (d). This work (298 K, 0.49 Torr, 0.06 cm^{-1}) vs data of Wennberg et al.[17] (294 K, 5 Torr, 0.028 cm^{-1}). We scaled the magnitude and added 0.01 cm^{-1} to the wavenumber scale for data from ref 17. The wavelength scale refers to vacuum.

The equilibrium constant for this reaction, $K_{\text{eq}} = [\text{NO}_2]^2/[\text{N}_2\text{O}_4] = 1.7 \times 10^{28} e^{-6643/T}$[molecules/cm^3], is known with better than 5% accuracy over the temperature range of interest.[27] Although the dimerization has a large effect on the *NO$_2$ concentration* in the cell for measurements done at or below 250 K (Table 2), the contribution of N$_2$O$_4$ to the *total absorbance* is negligible. Indeed, the dimer has a smooth absorption spectrum with a wing that only weakly penetrates into the spectral range investigated here.[28] Under no conditions did N$_2$O$_4$ contribute more than 2% to the total absorbance at 400 nm, where its contributions are expected to be largest (the interference is even smaller at 415 nm). Even though concentration of N$_2$O$_4$ increases quickly at lower temperatures, this is more than compensated by the exponential drop in N$_2$O$_4$ absorption cross sections above 400 nm with temperature. Therefore, we chose not to correct the absorbance for N$_2$O$_4$ contributions in this work.

The effect of dimerization on the NO$_2$ concentration can be quantitatively accounted for by combining the mass balance equation

$$\alpha = [\text{NO}_2] + 2[\text{N}_2\text{O}_4] = \delta[\text{M}]\frac{f_{\text{mix}}}{f_{\text{air}}} \qquad (3)$$

with the equilibrium constant, and solving for [NO$_2$]. Here, [M]

is the total density in the cell, which can be related to the experimentally measured temperature and pressure via the ideal gas law; f_{mix} and f_{total} are the NO_2 mixture flow and total flow, respectively; δ is the molar fraction of NO_2 in the bottle; and α is the hypothetical concentration of NO_2 in the absence of dimerization. The result for NO_2 density is

$$[NO_2] = \frac{K_{eq}}{4}\left(-1 + \sqrt{1 + \frac{8\alpha}{K_{eq}}}\right) \quad (4)$$

Propagation of errors through (eq 4) gives the following result

$$(\Delta[NO_2])^2 = \left(-\frac{K_{eq}}{4} + \frac{1}{4}\frac{K_{eq}^2 + 4\alpha K_{eq}}{\sqrt{K_{eq}^2 + 8\alpha K_{eq}}}\right)^2\left(\frac{\Delta K_{eq}}{K_{eq}}\right)^2 +$$
$$\left(\frac{\alpha K_{eq}}{\sqrt{K_{eq}^2 + 8\alpha K_{eq}}}\right)^2\left(\frac{\Delta\alpha}{\alpha}\right)^2$$

$$\frac{\Delta\alpha}{\alpha} = \sqrt{\left(\frac{\Delta\delta}{\delta}\right)^2 + \left(\frac{\Delta P}{P}\right)^2 + \left(\frac{\Delta T}{T}\right)^2 + \left(\frac{\Delta f_{total}}{f_{total}}\right)^2 + \left(\frac{\Delta f_{mix}}{f_{mix}}\right)^2}$$
$$(5)$$

In the high-temperature limit, where $\alpha \ll K_{eq}$, eq 5 reduces to the following

$$\frac{\Delta[NO_2]}{[NO_2]} =$$
$$\sqrt{\left(\frac{\Delta\delta}{\delta}\right)^2 + \left(\frac{\Delta P}{P}\right)^2 + \left(\frac{\Delta T}{T}\right)^2 + \left(\frac{\Delta f_{total}}{f_{total}}\right)^2 + \left(\frac{\Delta f_{mix}}{f_{mix}}\right)^2 + \left(\frac{2\alpha}{K_{eq}}\right)^2\left(\frac{\Delta K_{eq}}{K_{eq}}\right)^2}$$
$$(6)$$

In this limit, uncertainty in the equilibrium constant is strongly suppressed, and the error is dominated by uncertainties in the flow and molar fraction of NO_2 mixture. In the limit of low temperatures, where $\alpha \gg K_{eq}$, relative contributions from K_{eq} become much more important, but contributions from other variables are reduced by a factor of 2

$$\frac{\Delta[NO_2]}{[NO_2]} =$$
$$\frac{1}{2}\sqrt{\left(\frac{\Delta\delta}{\delta}\right)^2 + \left(\frac{\Delta P}{P}\right)^2 + \left(\frac{\Delta T}{T}\right)^2 + \left(\frac{\Delta f_{total}}{f_{total}}\right)^2 + \left(\frac{\Delta f_{mix}}{f_{mix}}\right)^2 + \left(\frac{\Delta K_{eq}}{K_{eq}}\right)^2} \quad (7)$$

The uncertainties in $[NO_2]$ are given in Table 2; these are calculated from eq 5 assuming conservative uncertainties (95% confidence limits) in δ, P, T, f_{mix}, f_{total}, and K_{eq} of 2.5%, 0.3%, 1%, 4%, 1%, and 5%, respectively. Large uncertainties associated with the flow terms incorporate both the accuracy of flow meter calibrations and small drifts in the flows through the needle valve over the course of the measurement (80 min per scan). For cases, where spectra were recorded using an undiluted flow of the NO_2 premix, the flow terms drop out and δ becomes the dominant contribution to the $[NO_2]$ uncertainty (Table 2).

The largest contributions to the *uncertainty in absorbance* came from the Xe arc light source drifts and fluctuations. We observed that the UV lamp intensity decreased with time with an initial $1/e$ time constant of approximately 2 days corresponding to the intensity drift of 2.1% per hour. The drift rate slowed considerably after 1 day of operation but was still noticeable. Spectral distribution of the lamp output was also slowly changing with time. Because the sample spectrum, I, and background spectrum, I_0, were not measured at the same time,

such slow drifts in the overall intensity and spectral distribution of the lamp radiation could produce a systematic error in absorbance if not properly compensated for. To minimize the drift effect, we recorded the empty cell scans both before and after each sample scan. The effective background spectrum was then calculated as a weighted average of the two adjacent background data sets assuming a linear variation in the lamp intensity with time. On the basis of the careful measurements of the intensity drift we could minimize the lamp drift error $\Delta I_0/I_0$ to less than 0.5% for all spectra.

How this uncertainty in I_0 translates into the error in absorbance depends on the value of absorbance itself. For the range of 415−525 nm, the NO_2 absorption cross section ranges between ca. 2×10^{-19} and 8×10^{-19} cm²/molecule.[2] In combination with the approximate range of NO_2 concentrations from Table 2, the range of absorbances utilized in this work corresponds to 0.1−0.9. In the small absorbance limit, error propagation gives the following approximate equation

$$\frac{|\Delta A_\lambda|}{A_\lambda} \approx \frac{\sqrt{2}}{A_\lambda} \times \frac{|\Delta I_0|}{I_0} \quad (8)$$

For the smallest cross sections recorded under conditions of the smallest NO_2 concentrations ($A_\lambda = 0.1$), the error in absorbance due to the lamp intensity drift alone can be as large as 7.0%. However, for 90% of the cross section data reported here (with $A_\lambda > 0.2$) the error amplification is not as dramatic ($\Delta A_\lambda/A_\lambda < 3.5\%$). Moreover, in the intermediate absorbance regime, the amplification factor proportional to $(A_\lambda)^{-1}$ disappears from eq 10 and relative uncertainties in I_0 and A_λ become roughly equal (i.e., 0.5%).

Short-term light source fluctuations and detector noise contributions to the uncertainty in A_λ were estimated directly from the spectra. For the spectral range of interest (415−525 nm) estimated RMS noise did not exceed 0.005 absorbance units translating to <2.5% uncertainty in absorbance for the majority of data reported here (with $A_\lambda > 0.2$). Together with the slow drift contribution, this produces a total uncertainty of < 4.3% for the measured absolute absorbances (for 90% of the reported data). As uncertainties in NO_2 concentrations did not exceed 5% (Table. 2), the reported cross sections should not deviate from the true values by more than 7%. Note that the error is likely to be largest at the edges of the spectral range studied here; 5% is probably a better estimate for the middle of the investigated range including the OMI validation window.

B. Beer−Lambert Law. Ideally, absorption cross sections should be measured by taking a series of spectra with varying concentrations of the analyte under identical P, T conditions, and fitting the resulting absorbances to the anticipated linear concentration dependence.[23] Following this procedure is especially important for molecules with highly structured absorption spectra, which are known to deviate from the Beer−Lambert law under conditions of low instrumental resolution. In addition, it minimizes the impact of potential impurities on the measurements. In Figure 5, we show our validation of the Beer−Lambert law at $T = 298$ K and $P = 10$ Torr. At this low pressure, broadening is dominated by the Doppler and radiative contributions. The vertical axis corresponds to the absorbance averaged over 22 800−23 100 cm⁻¹ spectral range. The uncertainties on the absorbance are larger than in our regular spectra from Table 2 because only two interferograms were co-added instead of 15, and the Xe lamp was on only for a few hours prior to the test. Nevertheless, the resulting absorbance is clearly a linear function of $[NO_2]$ with zero intercept. On the basis of this test,
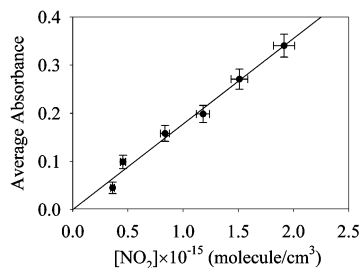
Figure 5. Beer−Lambert plot. The data were taken at $P_{total} = 10$ Torr and $T = 298$ K under 0.060 cm^{-1} resolution. The vertical axis corresponds to the absorbance averaged over $22\,800-23\,100$ cm^{-1} spectral range. The absorbance is seen to be directly proportional to the NO$_2$ concentration with zero offset.
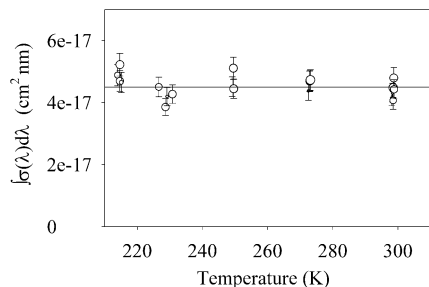

Figure 6. Comparison of integrated absolute cross sections with the literature values. The graph presents cross sections integrated over the range of 400−500 nm as a function of temperature. The size of the dots is logarithmically proportional to the pressure. As expected, there are no apparent correlations with either pressure or temperature. Note that our data are somewhat less reliable below 415 nm, which accounts for some of the observed scatter. Nevertheless, the average of all data (4.53×10^{-17} cm^2 nm) is in an excellent agreement with Orphal's recommendation for this range (4.50×10^{-17} cm^2 nm, shown by solid line).[3]

we felt that it was reasonable to assume that Beer−Lambert law applied under all other P, T conditions. Therefore, all absorption cross sections were calculated from eq 1, with measurements done at a single NO$_2$ concentration for any given P, T combination.

IV. Results and Discussion

A. Absolute Cross Sections. To verify how present data compare with previous measurements it is convenient to compare a quantity that is relatively insensitive to the experimental conditions such as pressure, instrumental resolution, and accuracy of wavelength calibration. Following Orphal's suggestion,[3] we chose to compare integrated cross sections over a fixed wavelength interval. Orphal analyzed all previous absorption spectroscopy data on NO$_2$ and deduced an integrated cross section of $\langle\sigma\rangle_{400-500} = \int_{400}^{500} \sigma(\lambda)d\lambda = 4.50 \times 10^{-17}$ cm^2 nm for the 400−500 nm range, with a standard deviation between different measurements (1σ) of 2.4%. Although our data become less accurate below 415 nm, we can still verify whether our absolute scale is in agreement with Orphal's inference.

In Figure 6, we present our measured $\langle\sigma\rangle_{400-500}$ values as a function of temperature and pressure. In agreement with previous observations,[3,29] the integrated cross sections do not display a visible temperature or pressure dependence. The experimental average of all our P, T data points is $\langle\sigma\rangle_{400-500} = 4.53 \times 10^{-17}$ cm^2 nm, which is within 1% of Orphal's recommendation. The agreement is even better (0.2%) if only the recent data from refs 12−14, 19, 22, 30, 31 are used for the integration yielding

a reference value of $\langle\sigma\rangle_{400-500} = 4.52 \times 10^{-17}$ cm^2 nm.[3] The scatter between individual measurements is amplified by the fact that we had to include the 400−415 range in the integration, where our cross sections are less certain. For example, if we use data corresponding to 435−500 nm window (the average of our integrated cross sections is $<\sigma>_{435-500} = 2.489 \times 10^{-17}$ cm^2 nm for this spectral range), the standard deviation between different P, T points (1σ) is reduced from 7.3% to 5.8% of the averaged value. The latter corresponds to a 2.5% confidence interval with 95% boundaries. As discussed above, most of this error is due to slow drifts in lamp UV intensity and in gas flows. Such drifts can be partly compensated for by adjusting the scale in such a way as to force the integrated cross sections in the 435−500 nm window to be the same ($<\sigma>_{435-500} = 2.489 \times 10^{-17}$ cm^2 nm). This correction has been applied to all cross section data reported in this work. Refer to the Supporting Information for actual cross section data.[32] Correction factors are given in the last column of Table 2.

The agreement in the wavelength dependence of the NO$_2$ absorption cross sections is also very good. For example, in Figure 4, we compare selected segments of the room-temperature NO$_2$ absorption spectrum with data of Vandaele et al.[13] recorded at a stated 0.1 cm^{-1} resolution but with a comparable wavelength point spacing (0.030 13 cm^{-1} vs 0.028 60 cm^{-1} in this work). One can see that the data agrees well both in the absolute magnitude and in wavelength dependence. Note that the effective resolution in ref 13 changes from 0.1 to 0.067 cm^{-1} if the resolution is re-defined as 1.207/[2 × MOPD] instead of 0.9/MOPD used in their paper (MOPD = maximum optical path difference). This is only 10% above our stated resolution of 1.207/[2 × MOPD] = 0.060 cm^{-1}. However, this small difference is enough to produce a visibly larger peak-to-valley contrast of the rotational structure in the low-pressure spectra (Figure 4a). The difference in contrast becomes much smaller at higher pressures when the resolution is no longer limited by the instruments (Figure 4b). Comparison with the data of Harder et al. recorded at 0.15 cm^{-1} resolution[12] reveals a similarly good level of agreement in wavelength (Figure 4c). The effect of the higher resolution on the spectrum is clearly observed; the spectrum from ref 12 is more convolved. The agreement between the present data set and spectra of refs 12,13 becomes somewhat less impressive at lower temperatures, but can still be characterized as very good.

We have also compared our data with measurements of Wennberg et al.[17] done at 0.028 cm^{-1} resolution (Figure 4d) between 441 and 452 nm. To achieve good agreement over the displayed range we had to scale the magnitude and add 0.01 cm^{-1} to the wavenumber scale for data from ref 17. Again, we find that the effect of the higher resolution (0.028 cm^{-1} vs 0.060 cm^{-1}) is to increase the amount of the observed structure in the cross section. In fact, some of the high-resolution features do not even show up in our 0.06 cm^{-1} spectrum because the resolution is still limited by the instrument (the spectrum from ref 17 is Doppler limited).

B. Pressure and Temperature Dependence. The visible spectrum of NO$_2$ is a conglomeration of thousands of individual lines from different overlapping vibronic bands, with a variety of transition strengths, collisional broadening parameters and temperature dependences of these parameters. In view of these factors, the NO$_2$ absorption cross sections are expected to have a nontrivial dependence on the environmental conditions. Specifically, the temperature and pressure impact the spectrum in several important ways. First of all, the Doppler widths directly depend on temperature

$$\text{HWHM}_{\text{Doppler}} = \nu_0 \sqrt{\frac{2\ln(2)kT}{mc^2}} \qquad (9)$$

In addition, the relative transition strengths, which are proportional to the Boltzmann population factors, are temperature dependent. The collisional contribution to the line width depends on both the temperature and pressure. Specifically, the simplest "strong" collision description of the pressure broadening effects predicts Lorentzian line profiles, with widths given by

$$\text{HWHM}_{\text{pressure}} \, [\text{s}^{-1}] = \frac{\text{collision frequency}}{2\pi} = \sigma P \sqrt{\frac{2}{\pi^3 \mu kT}} \qquad (10)$$

In formulas above, σ is the collision cross section (in m^2/molecule), μ is the reduced mass for NO_2 -air (in kg), m is the mass of NO_2 (in kg), k is the Boltzmann constant, and P is the total pressure (in Pa).

Recent studies of the NO_2 spectrum revealed a remarkably strong pressure dependence of the NO_2 absorption cross sections in the near-infrared and visible ranges.[12−15] With the high spectral resolution and broad P, T coverage of this work, the pressure effects are even more prominent. For example, In Figure 7a, a portion of the absorption spectrum that overlaps the OMI measurement window is shown for several different pressures at 273 K. The high-resolution noise-like structure clearly increases in amplitude as the total pressure is reduced. In Figure 7b an expanded window around 21 985 cm^{-1} is plotted for the same data set, offering a clearer look at the dramatic effect of pressure broadening on the spectrum.

Small relative intensity changes associated with temperature broadening of Boltzmann rotational state populations of NO_2 are detectable in the spectrum too, in agreement with the results of ref 15. On the contrary, the influence of temperature on the widths of high-resolution features is much less obvious, and it can only be discerned from a very careful line-by-line examination of the spectra. Such behavior can be rationalized with help of eqs 9−10. If, at any given pressure, the pressure induced width were proportional to $1/\sqrt{T}$ as in eq 10, and, the Doppler width (eq 9) is proportional to $\sqrt{T}$, then the temperature dependence of the total line width would be partly negated. For a temperature range between 300 and 210 K, the Lorentz width would vary by 20% at most. Given the congestion of the spectrum, it is very difficult to quantify the temperature dependence of the air-broadened widths.

Observational work needs absorption cross sections of NO_2 for all possible conditions relevant to atmospheric chemistry. Unfortunately, the spectroscopy of NO_2 is not understood well enough to model the spectrum on a line-by-line basis. Another approach[14,15] to the problem is to use a high quality experimental spectrum (or spectra) of NO_2 as a template, from which the entire absorption spectrum at any given resolution, temperature, and pressure can be quantitatively predicted with a semiempirical model. For example, one could choose two high-resolution reference spectra recorded at the lowest possible pressure at two limiting temperatures, which surround the atmospheric 210−300 K range, and produce spectra at other P, T conditions using a combination of simple convolutions and interpolations. Such an approach was used successfully in ref 15 to parametrize the visible absorption cross sections of NO_2 at 0.1 cm^{-1} (and lower) resolution. A similar Lorentzian convolution approach was used to reproduce 1000 mbar spectra from 100 mbar spectra at 0.5 cm^{-1} resolution.[14] In this work, we investigated whether this approach can be sufficiently
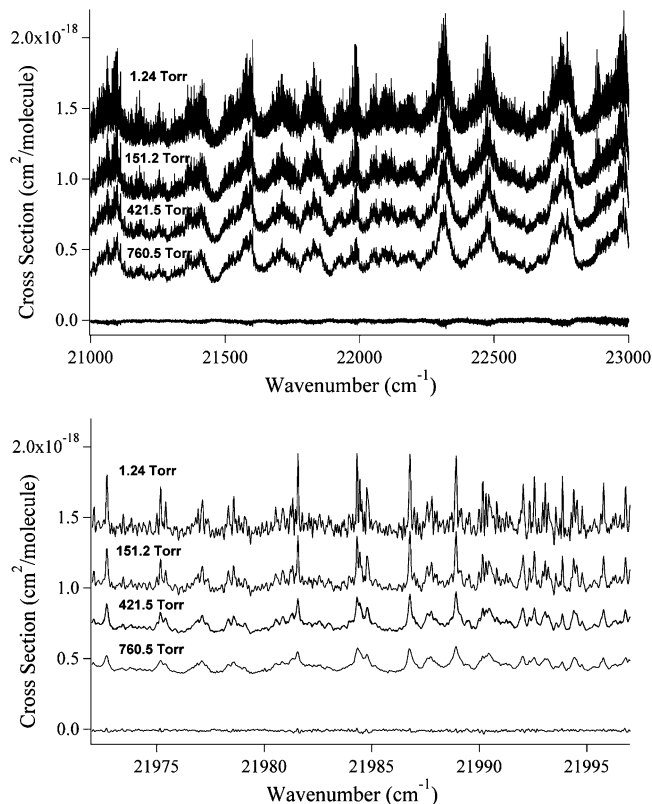

Figure 7. Effect of total pressure on the observed cross sections in the range including OMI validation window. Top: The relative amplitude of the high-resolution structure decreases dramatically with pressure (273 K data shown; P = 1.24, 151.2, 421.5, 760.5 Torr from top to bottom). Traces are offset for clarity; absolute scale applies only to the 760.5 Torr trace. The lowest trace is the difference between the 421.5 Torr data and convolution of the 1.24 Torr data with a Lorentzian filter with an effective width of HWHM = 0.058 cm^{-1} (the best least-squares fitted width for this particular case). Bottom: Same data as in the top panel shown in a narrower frequency interval.

accurate to reproduce our higher resolution spectra with acceptable precision.

At any given temperature, the ambient pressure will only affect the collisional contribution to line widths because, in the zero-order approximation, transition strengths, Doppler widths, and natural widths are all pressure independent. Therefore, one would expect that NO_2 spectra recorded at finite pressures can be obtained via a convolution of a "zero" pressure spectrum recorded at the same temperature with an appropriate collision-broadened line shape. (Note that the pressure broadening occurs in the cross-section space, so by "spectrum" we mean absorption cross sections, not transmittance). Line broadening parameters have been measured for NO_2 in the infrared and near-infrared ranges,[33−37] and they are known to depend slightly on both the rotational and vibrational states of NO_2. In the visible range, the pressure-broadening parameters have not been explicitly measured, but the analysis of pressure-dependent NO_2 absorption cross sections done in ref 15 suggests that the effective pressure-broadening widths increase systematically with the excitation energy. The main question is whether a single pressure-broadening parameter would be sufficient for correctly predicting the spectrum over the limited frequency range used in this work.

As seen in Figures 7 and 8, a simple Lorentzian convolution works quite well for all atmospherically relevant pressures at 0.060 cm^{-1} resolution. To generate Figure 8, an absorption cross section spectrum recorded at the lowest available pressure (0.5−5 Torr; depending on temperature) was convolved with a
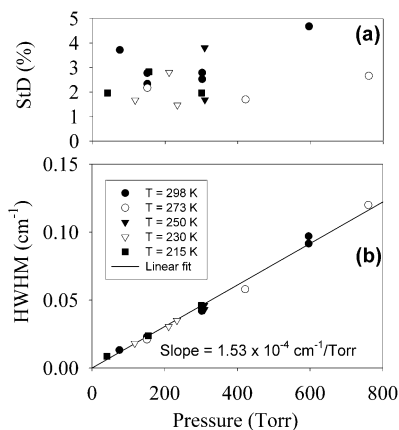
Figure 8. Results of the Lorentzian convolution of low-pressure cross sections of NO$_2$ into high pressure ones. The convolution used Lorentzian line half-width as an adjustable parameter to minimize least-squares deviations (panel a) between the convoluted and experimentally measured cross sections in the 20 900−23 100 cm^{-1} interval. Optimal line widths for different temperatures (panel b) have similar pressure dependence with a common slope of 1.53(4) × 10^{-4} cm^{-1}/Torr or 0.116 ± 0.003 cm^{-1}/atm (uncertainties are 95% confidence intervals). An example of a convoluted spectrum is shown in Figure 7.

Lorentzian line shape filter. The Lorentzian width was treated as an adjustable parameter. The convolution aimed at minimizing least-squares deviations between the calculated and experimentally measured NO$_2$ cross sections in the 20 900−23 100 cm^{-1} interval, where the cross sections have rich structure and are characterized by high measurement accuracy. In Figure 7b, the convoluted spectrum is superimposed on the experimental spectrum, and the two traces are, indeed, nearly indistinguishable. Furthermore, as seen in Figure 8a, the resulting standard deviations (1σ) are well within our experimental accuracy.

In Figure 8b, the resulting Lorentzian widths are shown as a function of the total pressure. In agreement with eq 10, the widths depend linearly on pressure. Somewhat unexpectedly, the influence of temperature on the observed slopes is marginal. All the temperature-dependence data lie on the same line with a common slope of $\gamma = 0.116 \pm 0.003$ cm^{-1}/atm (HWHM; uncertainties are 95% confidence intervals). Using eq 10, the slope translates to an effective collision cross section of ≈150 Å^2, which is larger than expected from a hard-sphere collision perspective but probably quite reasonable for de-phasing in NO$_2$ − N$_2$/O$_2$ collisions.

The present findings appear to disagree with the results of Vandaele et al.,[15] who reported smaller pressure-broadening effects and a measurable temperature dependence for the Lorentzian widths. Specifically, they represented γ as $\gamma_0 \times (T_0/T)^n$, where $T_0 = 298$ K is a reference temperature, and reported $\gamma_0 = 0.081$, $n = 0.8$ as the best fit to the data from different workers in the 14 000−23 000 cm^{-1} range. For the sake of consistency, we reanalyzed the visible absorption cross section data of ref 15 with our own code and reproduced their findings. The authors of ref 15 did find that the effective pressure-broadening width increases to $\gamma_0 = 0.1$, and the power decreases to $n = 0.55$ when only data near 22 000 cm^{-1} are used in the analysis, which is in a better agreement with the present results ($\gamma_0 = 0.116$, $n \approx 0$). The most plausible explanation for the remaining discrepancy could be associated with the slightly lower effective resolution of data from ref 15. Specifically, one would expect that the apparent pressure broadening parameter must get smaller as the instrumental resolution is degraded. However, Voigt et al.[14] used a similar convolution approach at an even lower resolution (0.5 cm^{-1}) to reproduce 1000 mbar spectra from 100
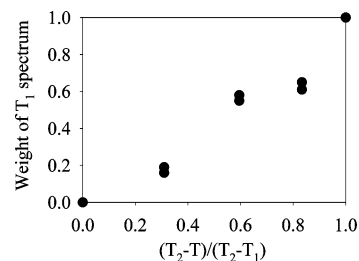

Figure 9. Testing the linearity assumption for the temperature dependence of NO$_2$ absorption cross sections. Low-pressure cross sections recorded at $T_1 = 215$ K and $T_2 = 298$ K are used as references, and data at intermediate temperatures T are fitted to $\sigma(\bar{\nu},T) = \omega(T)\sigma(\bar{\nu},T_1) + (1 - \omega(T))\sigma(\bar{\nu},T_2)$ using $\omega(T)$ as adjustable parameters. Two points per T arise from using either $P = 0.49$ Torr or $P = 1.99$ Torr data for T_2. Although the quality of the fits is close to that obtained in the pressure broadening convolutions (Figure 7), $\omega(T)$ is obviously not a linear function of $[T_2 - T]/[T_2 - T_1]$ implying that the linear assumption is not valid over the entire 210−300 K range.

mbar spectra. They obtained $\gamma_0 = 0.134$, $n = 1.03$, which is *higher* than reported by other groups. Obviously, more high resolution work on the pressure broadening effects in the visible spectrum of NO$_2$ is required. Presently available data suggest that the observed pressure broadening parameters are both spectral range and resolution dependent.

We demonstrated that, for any given temperature, one requires a single low-pressure NO$_2$ experimental spectrum to successfully reproduce spectra at all higher pressures via a simple convolution (however, the pressure-broadening parameters required for this purpose depend on the resolution and on the frequency range of interest). Obviously, one cannot hope to use a similar convolution approach to model the temperature dependence. A reduction in temperature will cause lines originating from low energy ro-vibrational states to grow and lines from high energy states to diminish in amplitude. Because lines from different vibronic transitions strongly overlap, the temperature effect will have a highly irregular dependence on the wavelength (see Figure 4 of ref 15 as an example of such dependence).

However, for a limited range of temperatures, it may be possible to reproduce the unknown spectrum at desired temperature T as a weighted average of two known limiting spectra at temperatures T_1 and T_2, such that $T_1 < T < T_2$. We attempted this approach with the low-pressure spectra, using $T_1 = 215$ K and $T_2 = 298$ K as references. Spectra at intermediate temperatures were least-squares fitted to the expression

$$\sigma(\bar{\nu},T) = \omega(T)\sigma(\bar{\nu},T_1) + (1 - \omega(T))\sigma(\bar{\nu},T_2) \quad (11)$$

where $\omega(T)$ is an adjustable parameter. This approach is fully equivalent to the linear temperature dependence approximation used by Vandaele at al.[15]

$$\sigma(\bar{\nu},T) = \sigma(\bar{\nu},T_1) + \alpha(\bar{\nu})(T - T_1) \quad (12)$$

(they used $T_1 = 273$ K as reference) if one puts $\omega(T) = [T_2 - T]/[T_2 - T_1]$ and $\alpha(\bar{\nu}) = [\sigma(\bar{\nu},T_2) - \sigma(\bar{\nu},T_1)]/[T_2 - T_1]$. In their analysis, Vandaele et al.[15] assumed that simple linear approximation (eq 12) would adequately describe the temperature dependence of the NO$_2$ absorption cross sections for the low-pressure data for a very broad frequency range (13 000−25 000 cm^{-1} at 0.1 cm^{-1} resolution and 13 000−42 000 cm^{-1} at 2 cm^{-1} resolution). On the basis of this assumption they came up with a recommended value of $\alpha(\bar{\nu})$ required to predict low-pressure spectra at any temperature from the reference spectrum at 273 K. Our data suggest that the linear assumption is not valid even for the narrower frequency range used in this work. Although

4872 *J. Phys. Chem. A, Vol. 108, No. 22, 2004*

Nizkorodov et al.

we could find parameters $\omega(T)$ that reproduce the intermediate spectra with the standard deviation below 5% for the range of 19 000 to 23 100 cm^{-1}, the weights did not obey the anticipated linear temperature dependence (Figure 9). This means that linear temperature interpolation of cross sections should be used with great caution. Whereas it works quite well for the lower resolution data,[15] deviation from this simple model become substantial under higher resolution conditions of this work. We note that better interpolation results are obtained if T_1 and T_2 are closer to each other, but a successful parametrization of the temperature dependence for high-resolution absorption cross sections of NO$_2$ clearly requires more work.

V. Conclusions

In summary, we have presented new measurements of high-resolution (0.060 cm^{-1}) absorption cross sections of air-broadened NO$_2$ in the 415−525 nm region with the frequency accuracy of 0.011 cm^{-1} (2.8 $\times$ 10^{-4} nm at 500 nm) and precision is 0.0022 cm^{-1} throughout the investigated wavelength range. These were obtained on a broad Temperature−Pressure grid that closely follows conditions found in the troposphere and stratosphere, thus minimizing the need for complicated and potentially unreliable interpolations of the cross section data in atmospheric remote sensing applications. Analysis of our sources of error indicated that the cross sections should be accurate to better than 7% (2σ), and the integrated intensity is within 0.2% of other reported values. We have shown that a simple Lorentzian broadening model, with linear dependence of the Lorentz width on pressure, provides an adequate description of pressure broadening effects in NO$_2$. However, the observed discrepancy between the magnitude and temperature dependence of the pressure broadening parameters in the visible and near-IR spectral ranges clearly needs further study. We have also shown that temperature effects on the high-resolution absorption cross sections of NO$_2$ cannot be accurately reproduced using linear interpolation between spectra recorded at different temperatures (even though this method works well for lower resolution data).[15] Because the complexity of the temperature dependence of NO$_2$ absorption cross sections remains the main obstacle for a reliable NO$_2$ spectrum parametrization, we suggest that future measurements should focus on recording high-quality spectra at the lowest achievable pressure at frequently spaced (one spectrum every 5 K) temperatures using a Doppler limited resolution (fwhm < 0.036 cm^{-1}).

Supporting Information Available: Absorption cross sections of NO$_2$ are available free of charge via the Internet at http://pubs.acs.org.

References and Notes

(1) Velders, G. J. M.; Granier, C.; Portmann, R. W.; Pfeilsticker, K.; Wenig, M.; Wagner, T.; Platt, U.; Richter, A.; Burrows, J. P. *J. Geophys. Res. -Atmos.* **2001**, *106*, 12 643.

(2) Kirmse, B.; Delon, A.; Jost, R. *J. Geophys. Res.-Atmos.* **1997**, *102*, 16 089.

(3) Orphal, J. *J. Photochem. Photobiol. A-Chem.* **2003**, *157*, 185−209.

(4) Jortner, J.; Rice, S. A.; Hochstrasser, R. M. *Adv. Photochem.* **1969**, *7*, 149.

(5) Douglas, A. E. *J. Chem. Phys.* **1966**, *45*, 1007.

(6) Bixon, M.; Jortner, J. *J. Chem. Phys.* **1969**, *50*, 3284.

(7) Gillispie, G. D.; Khan, A. U.; Wahl, A. C.; Hosteny, R. P.; Krauss, M. *J. Chem. Phys.* **1975**, *63*, 3425.

(8) Gillispie, G. D.; Khan, A. U. *J. Chem. Phys.* **1976**, *65*, 1624.

(9) Smalley, R. E.; Ramakrishna, B. L.; Levy, D. H.; Wharton, L. *J. Chem. Phys.* **1974**, *61*, 4363.

(10) Hiraoka, S.; Shibuya, K.; Obi, K. *J. Mol. Spectrosc.* **1987**, *126*, 427.

(11) Hsu, D. K.; Monts, D. L.; Zare, R. N. Spectral Atlas of Nitrogen Dioxide 5530 to 6480 nm; Academic Press: New York, 1978.

(12) Harder, J. W.; Brault, J. W.; Johnston, P. V.; Mount, G. H. *J. Geophys. Res.-Atmos.* **1997**, *102*, 3861.

(13) Vandaele, A. C.; Hermans, C.; Fally, S.; Carleer, M.; Colin, R.; Merienne, M. F.; Jenouvrier, A.; Coquart, B. *J. Geophys. Res.-Atmos.* **2002**, *107*, 4348.

(14) Voigt, S.; Orphal, J.; Burrows, J. P. *J. Photochem. Photobiol. A.* **2002**, *149*, 1.

(15) Vandaele, A. C.; Hermans, C.; Fally, S.; Carleer, M.; Merienne, M. F.; Jenouvrier, A.; Coquart, B.; Colin, R. J. *Quant. Spectrosc. Radiat. Transf.* **2002**, *76*, 373.

(16) Orphal, J.; Chance, K. J. *Quant. Spectrosc. Radiat. Transf.* **2003**, *82*, 491.

(17) Wennberg, P. O.; Brault, J. W.; Hanisco, T. F.; Salawitch, R. J.; Mount, G. H. *J. Geophys. Res.-Atmos.* **1997**, *102*, 8887.

(18) Yoshino, K.; Esmond, J. R.; Parkinson, W. H. *Chem. Phys.* **1997**, *221*, 169.

(19) Vandaele, A. C.; Hermans, C.; Simon, P. C.; VanRoozendael, M.; Guilmot, J. M.; Carleer, M.; Colin, R. *J. Atmos. Chem.* **1996**, *25*, 289.

(20) Frost, G. J.; Goss, L. M.; Vaida, V. *J. Geophys. Res.-Atmos.* **1996**, *101*, 3869.

(21) Coquart, B.; Jenouvrier, A.; Merienne, M. F. *J. Atmos. Chem.* **1995**, *21*, 251.

(22) Merienne, M. F.; Jenouvrier, A.; Coquart, B. *J. Atmos. Chem.* **1995**, *20*, 281.

(23) Schneider, W.; Moortgat, G. K.; Tyndall, G. S.; Burrows, J. P. *J. Photochem. Photobiol. A.* **1987**, *40*, 195.

(24) Kasha, M. *J. Opt. Soc. Am.* **1948**, *38*, 929.

(25) Gerstenkorn, S.; Luc, P. *J. Physique (Paris)* **1985**, *46*, 867.

(26) Brown, L. R.; Margolis, J. S.; Norton, R. H.; Stedry, B. D. *Appl. Spectrosc.* **1983**, *37*, 287.

(27) Roscoe, H.; Hind, A. K. *J. Atmos. Chem.* **1993**, *16*, 257.

(28) Bass, A. M.; Ledford, A. E.; Laufer, A. H. *J. Res. Natl. Bur. Stand: A. Phys. Chem.* **1976**, *80A*, 143.

(29) Harwood, M. H.; Jones, R. L. *J. Geophys. Res.-Atmos.* **1994**, *99*, 22 955.

(30) Merienne, M. F.; Jenouvrier, A.; Coquart, B.; Lux, J. P. *J. Atmos. Chem.* **1997**, *27*, 219.

(31) Vandaele, A. C.; Hermans, C.; Simon, P. C.; Carleer, M.; Colin, R.; Fally, S.; Merienne, M. F.; Jenouvrier, A.; Coquart, B. *J. Quant. Spectr. Rad. Transf.* **1998**, *59*, 171.

(32) See the Supporting Information.

(33) Bouazza, S.; Kissel, A.; Sumpf, B.; Kronfeldt, H. D. *J. Mol. Spec.* **1999**, *198*, 18.

(34) Gianfrani, L.; Santovito, M. R.; Sasso, A. *J. Mol. Spec.* **1997**, *186*, 207.

(35) Dana, V.; mandin, J. Y.; Allout, M. Y.; Perrin, A.; Regalia, L.; Barbe, A.; Plateaux, J. J.; Thomas, X. *J. Quant. Spectrosc. Radiat. Transf.* **1997**, *57*, 445.

(36) Pustogov, V. V.; Kuhnemann, F.; Sumpf, B.; Heiner, Y.; Herrmann, K. *J. Mol. Spec.* **1994**, *167*, 288.

(37) Devi, V. M.; Fridovich, B.; Jones, G. D.; Snyder, D. G. S.; Neuendorffer, A. *Appl. Opt.* **1982**, *21*, 1537.